Electronic Supplementary Material (ESI) for Journal of Materials Chemistry A.

Supplementary Information

Surfactants-mediated synthesis of single-crystalline Bi_3O_4Br nanorings with enhanced photocatalytic activity

Xuyang Xiong,[a] Tengfei Zhou,[b] Xiufan Liu,[a] Shuoping Ding,[a] and Juncheng Hu*[a]

[a]Key Laboratory of Catalysis and Materials Science of the State Ethnic Affairs Commission & Ministry of Education South-Central University for Nationalities Wuhan 430074, PR China.

[b]Institute for Superconducting and Electronic Materials, School of Mechanical, Materials and Mechatronics Engineering, Faculty of Engineering and Information Science. University of Wollongong, North Wollongong, New South Wales, 2500, Australia.

*Corresponding author: jchu@mail.scuec.edu.cn (Juncheng Hu).

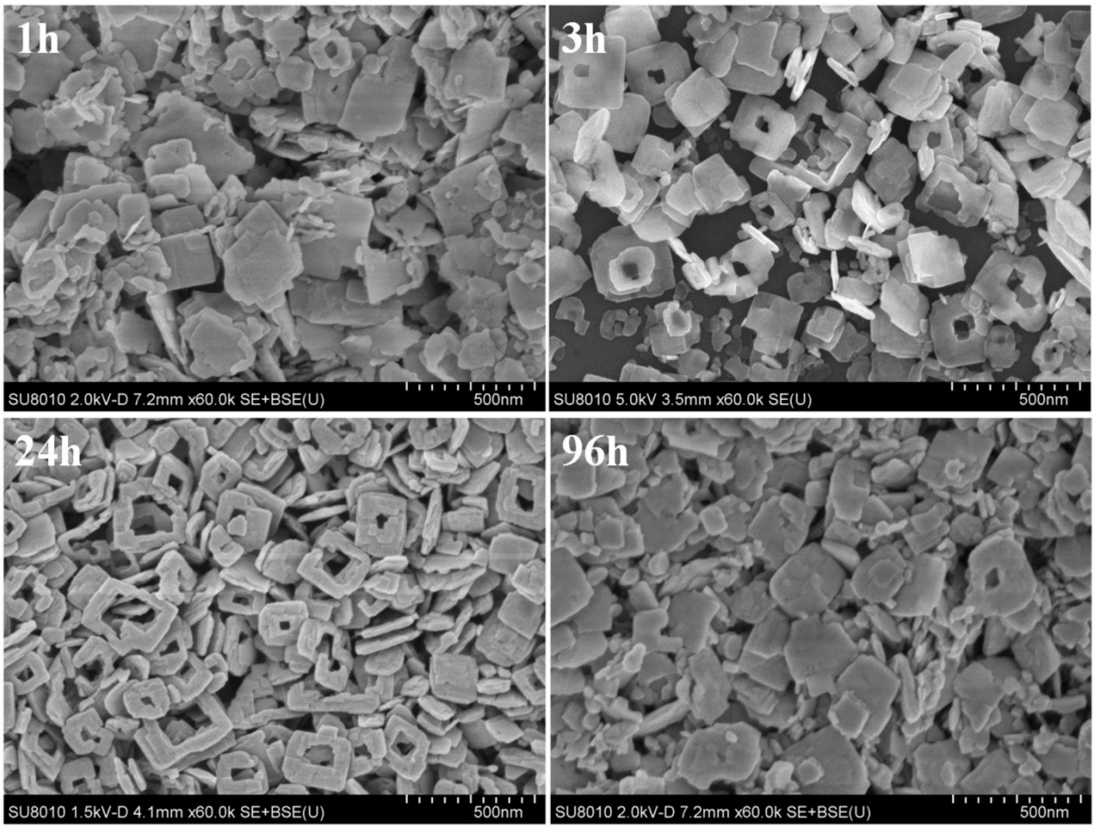

Fig. S1 SEM images of the samples (1 h, 3 h, 24 h, 96 h).

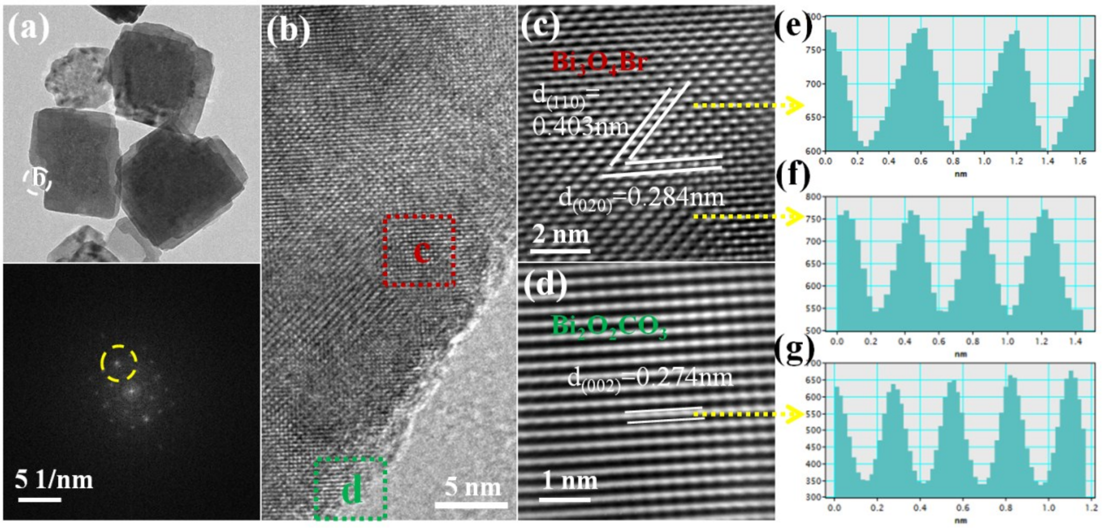

Fig. S2 TEM, HRTEM, FFT images of the samples obtained at 1 h.

We carefully examined the edge regions of the samples obtained at 1h (Fig. S2a). As shown in Fig. S2b-g, clearly lattice fringes of (110), (020) planes of Bi_3O_4Br and (002) planes of $Bi_2O_2CO_3$ have been observed. The corresponding FFT images further convinced the co-exist of Bi_3O_4Br and $Bi_2O_2CO_3$ species in the single nanoplates. Thus, the samples obtained at 1 h were further labeled as BOC/BOB NPs.

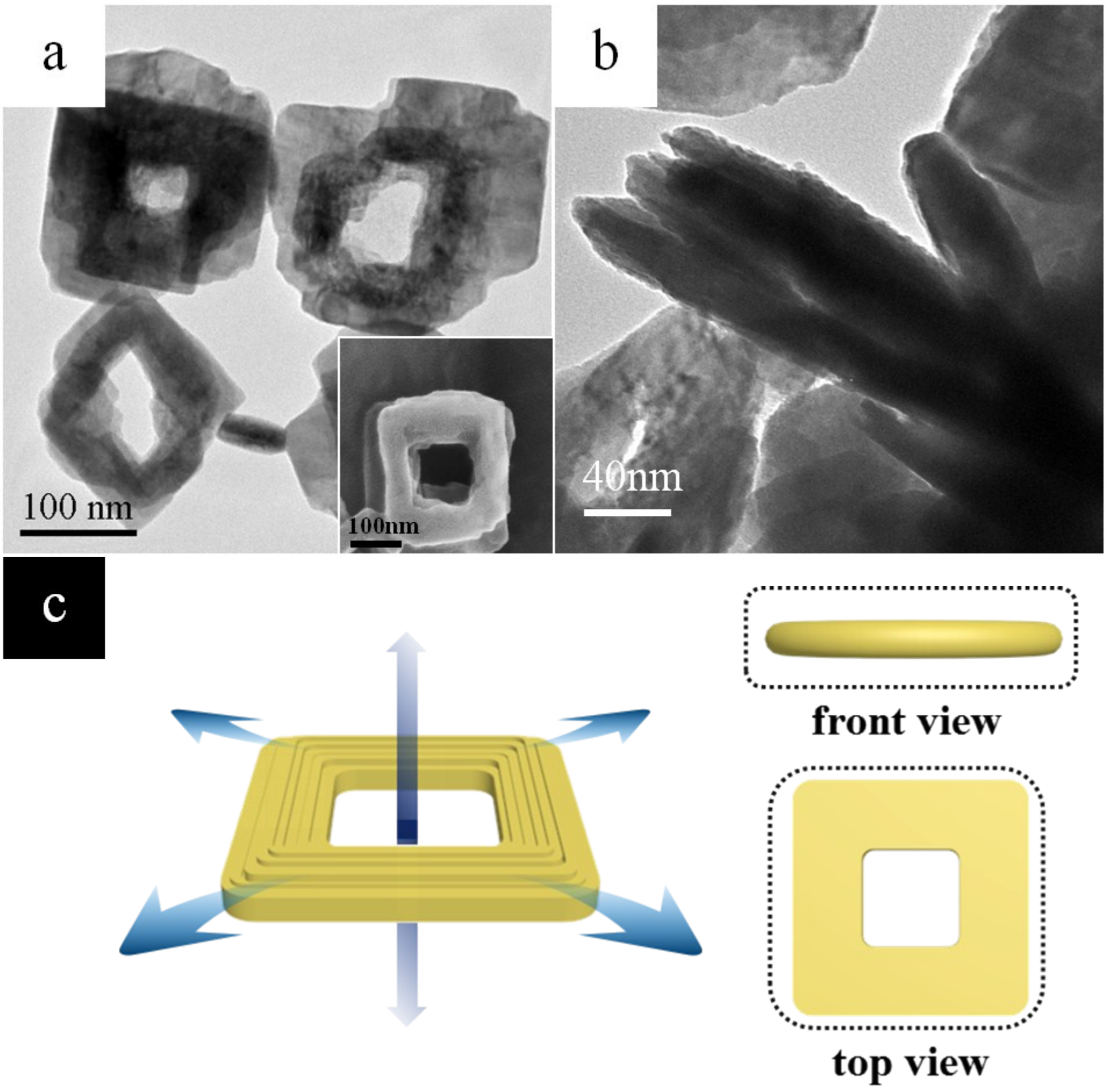

Fig. S3 The detailed morphology of Bi_3O_4Br nanorings. (a) top view of the nanorings, (b) side view of the nanorings, (c) Schematic illustration of the nanorings.

As shown in Fig. S3a, the exterior length is about 150-200 nm, interior length is about 50-100 nm and the thickness is about 30-40 nm (Fig. S3b). The general structure is also shown in Fig. S3c.

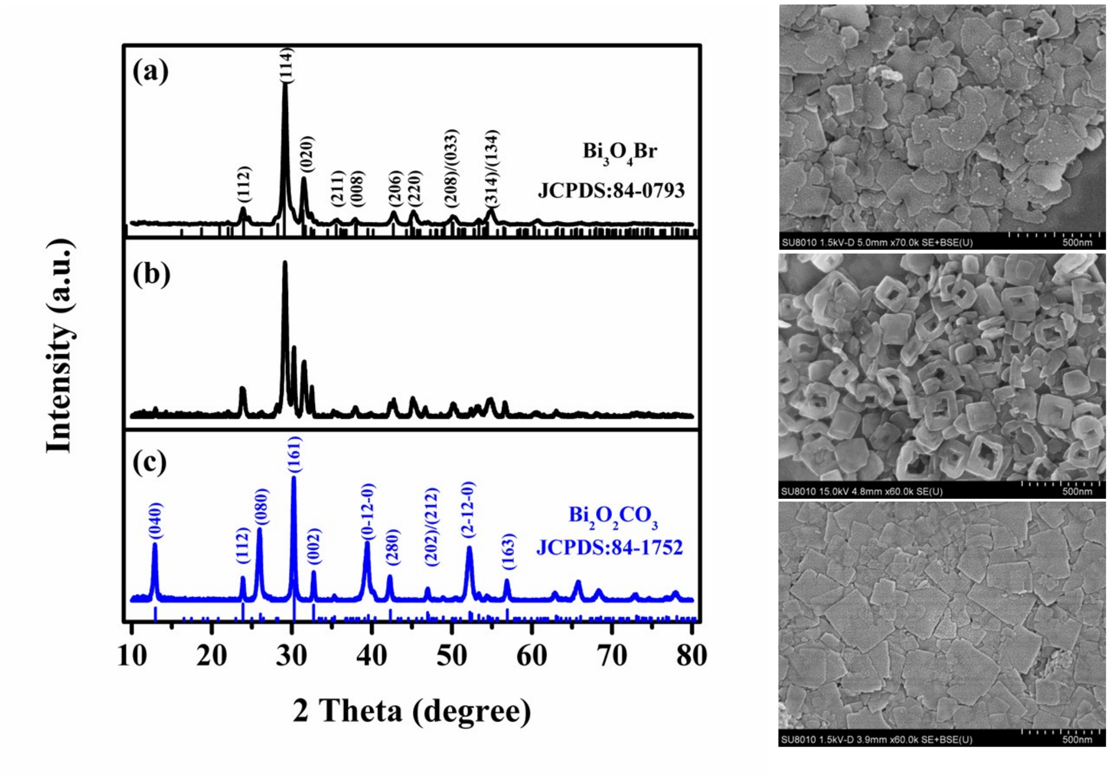

Fig. S4 XRD and SEM images of the samples prepared at 3 h with (a) only CTAB. (b) PVP and CTAB. (c) only PVP.

As shown in Fig. S4a-c, both CTAB and PVP plays the pivotal role in forming the ringlike strcture. Without PVP, the samples were pure Bi_3O_4Br. Without CTAB, the sample were pure $Bi_2O_2CO_3$. Confirmed that the PVP served as carbon source in the reaction which is the origin of CO_3^{2-} anions. This was also reported by Peng et al.[1] Generally, PVP is a widely used surfactant. Divided by their average molecular weight, they could by separated as K-30, K-60, K-90. Here, we used K-30.

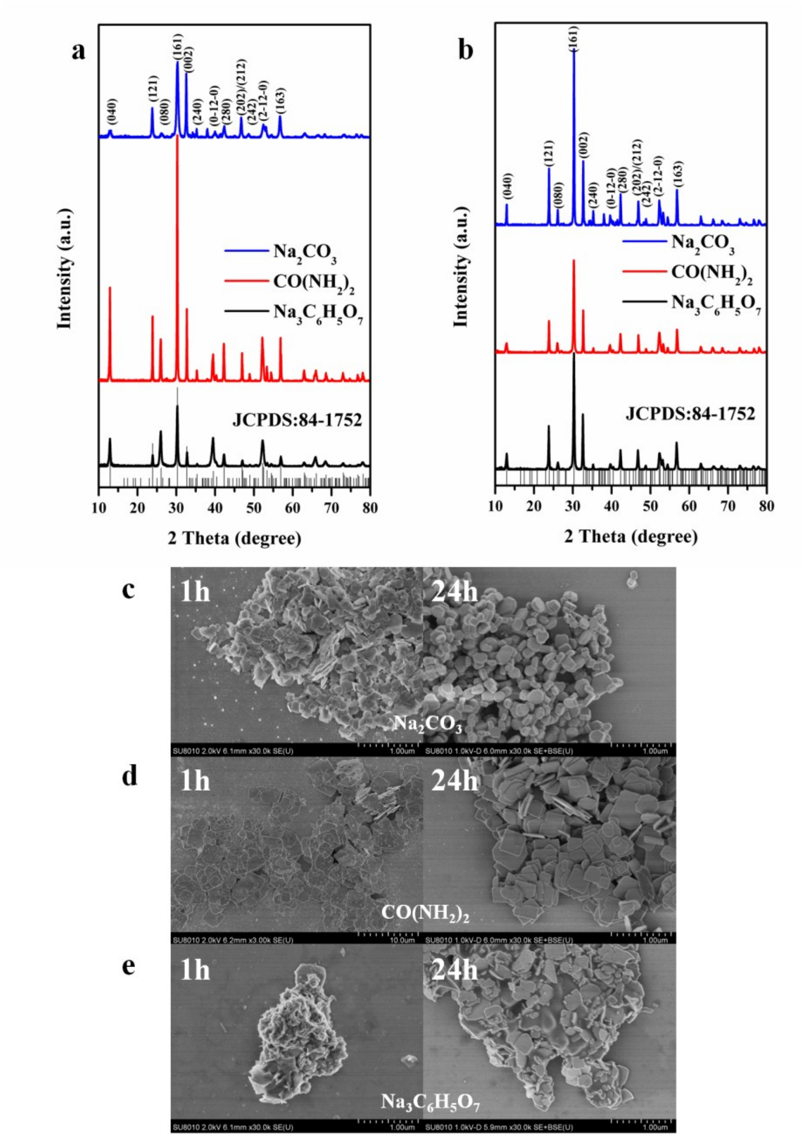

Fig. S5 XRD and SEM images of the samples prepared using other carbon source instead of PVP (a) XRD patterns of the samples obtained at 1 h. (b) XRD patterns of the samples obtained at 24 h. (c) SEM images of samples using Na_2CO_3 instead of PVP. (d) SEM images of samples using $CO(NH_2)_2$ instead of PVP. (e) SEM images of samples using $Na_3C_6H_5O_7$ instead of PVP.

As shown in Fig. S5a,b, the XRD patterns of these samples obtained in 1 h and 24 h could be well indexed as pure Bi_3O_4Br (JCPDS: 84-1752). The corresponding morphology of these samples were shown in Fig. S5c-e. Based on these experimental results, we could reasonably concluded that the morphology and chemical composition could not change from 1 h to 24 h. Therefore, merely replacing PVP by the same amount of Na_2CO_3, $Na_3C_6H_5O_7$ and $CO(NH_2)_2$, the samples obtained at 1 h was pure $Bi_2O_2CO_3$ nanostructures and remained stable at 24 h. This observation also revealed that the unique role of PVP molecules compared with other common carbon sources.

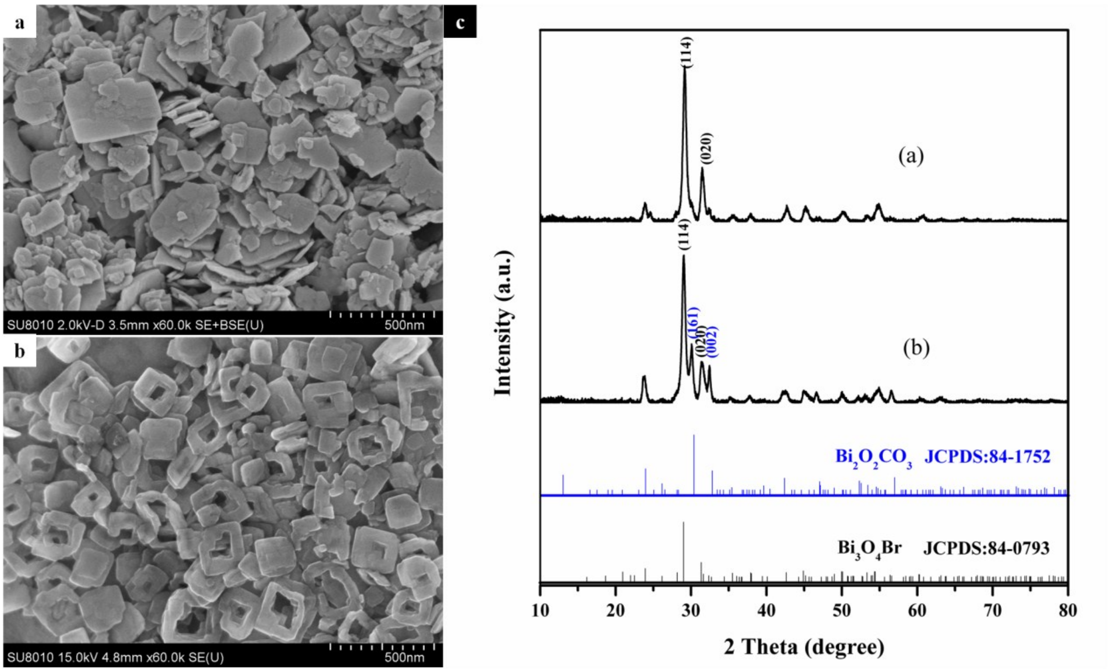

Fig. S6 SEM and XRD patterns of the samples obtained 3 h with (a) NaBr and (b) CTAB. The other reaction parameters are unchanged.

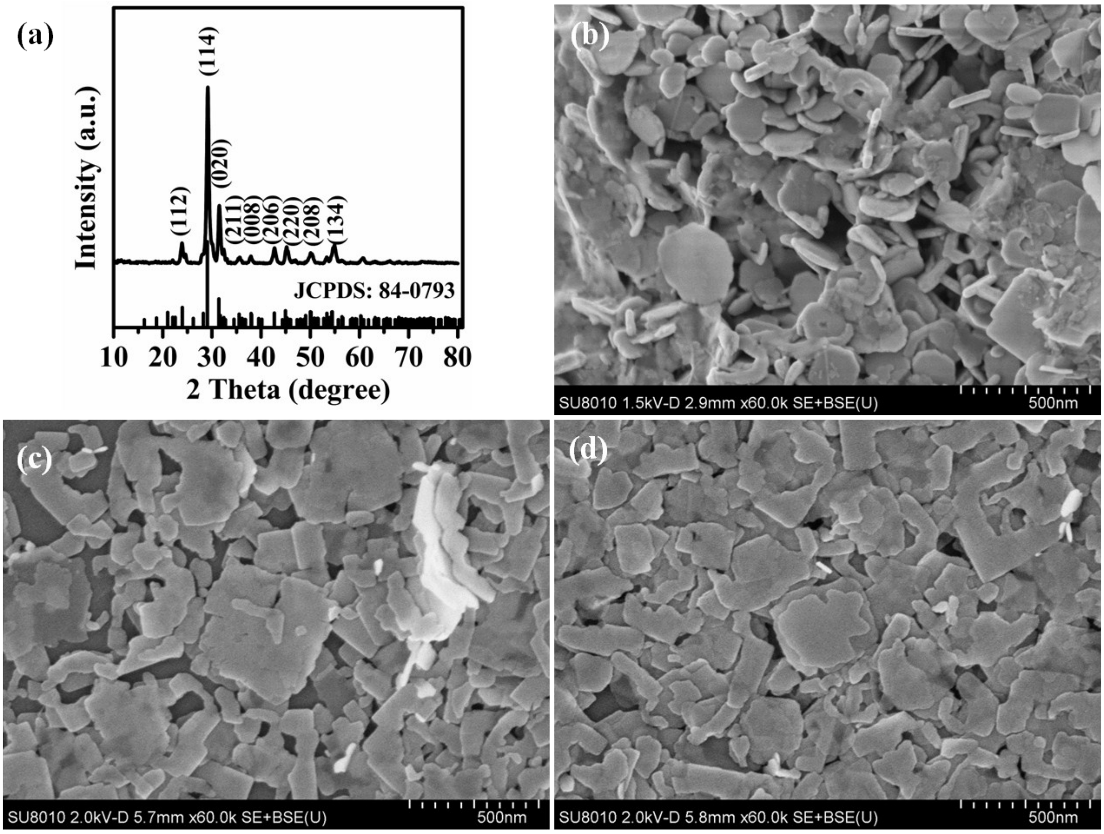

Fig. S7 XRD and SEM images of the rinsed samples obtained at (a,b) 1 h; (c) 3 h; (d) 24 h.

We used the samples obtained at 1 h as the templates. After carefully rinsed these samples to remove the PVP and CTAB, we further added them into the reaction system. From these experimernts, no nanorings were observed, indicating that the PVP and CTAB might influence the etching pathways of the samples.

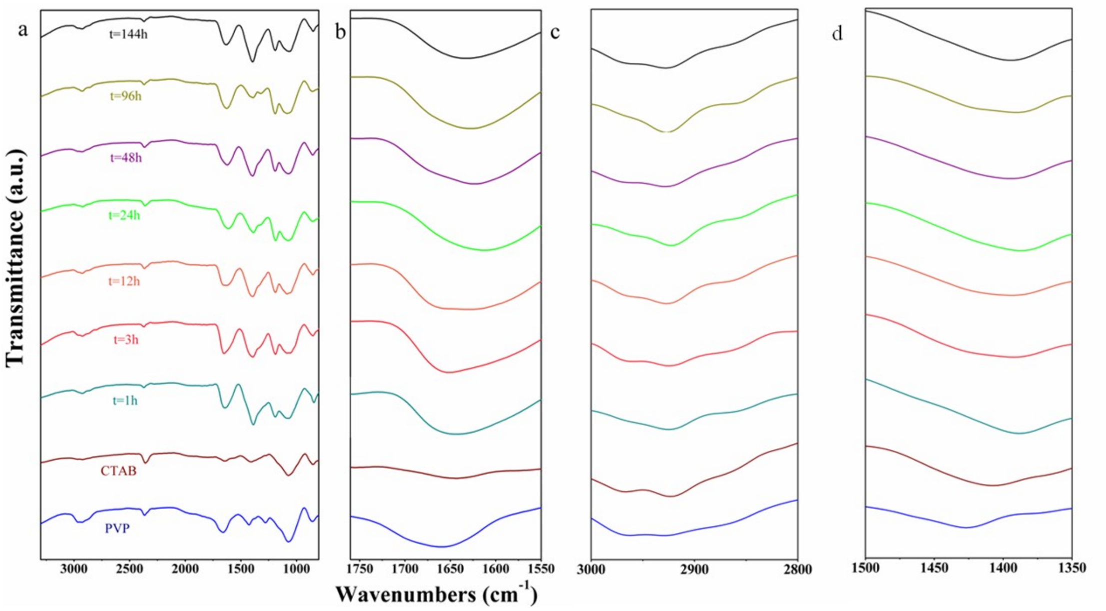

Fig. S8 FTIR of pure PVP, CTAB and the samples obtained from 1 to 144 hours.

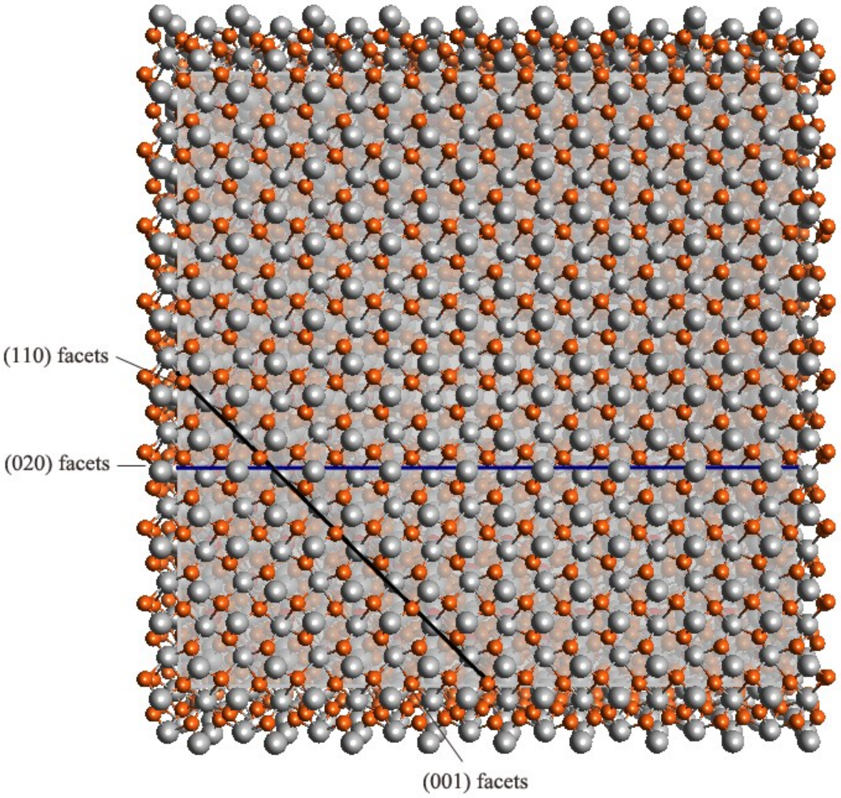

Fig. S9 Atom distribution and the relative position of crystalline facets of (001), (020), (110).

The angle between different facets of orthorhombic crystal was calculated by such formule:

$$\cos(\theta) = \frac{\frac{h_1h_2}{a^2}+\frac{k_1k_2}{b^2}+\frac{l_1l_2}{c^2}}{\sqrt{\left(\frac{h_1^2}{a^2}+\frac{k_1^2}{b^2}+\frac{l_1^2}{c^2}\right)\left(\frac{h_2^2}{a^2}+\frac{k_2^2}{b^2}+\frac{l_2^2}{c^2}\right)}}$$

Here, a=5.705 Å, b=5.694 Å, c=18.949 Å for orthorhombic Bi_3O_4Br; h_1, k_1, l_1 are the "Miller Index" of facets "1"; h_2, k_2, l_2 are the "Miller Index" of facets "2"; and θ is the angle between these two different crystal facets. As a result, the angle between (020) and (110) facets of Bi_3O_4Br was 45.24°. Besides, (001) facets was vertical to both facets, thus the dominate exposed facets of the Bi_3O_4Br nanorings was (001) facets. The relative position of these crystal planes was displayed in Fig. S9.

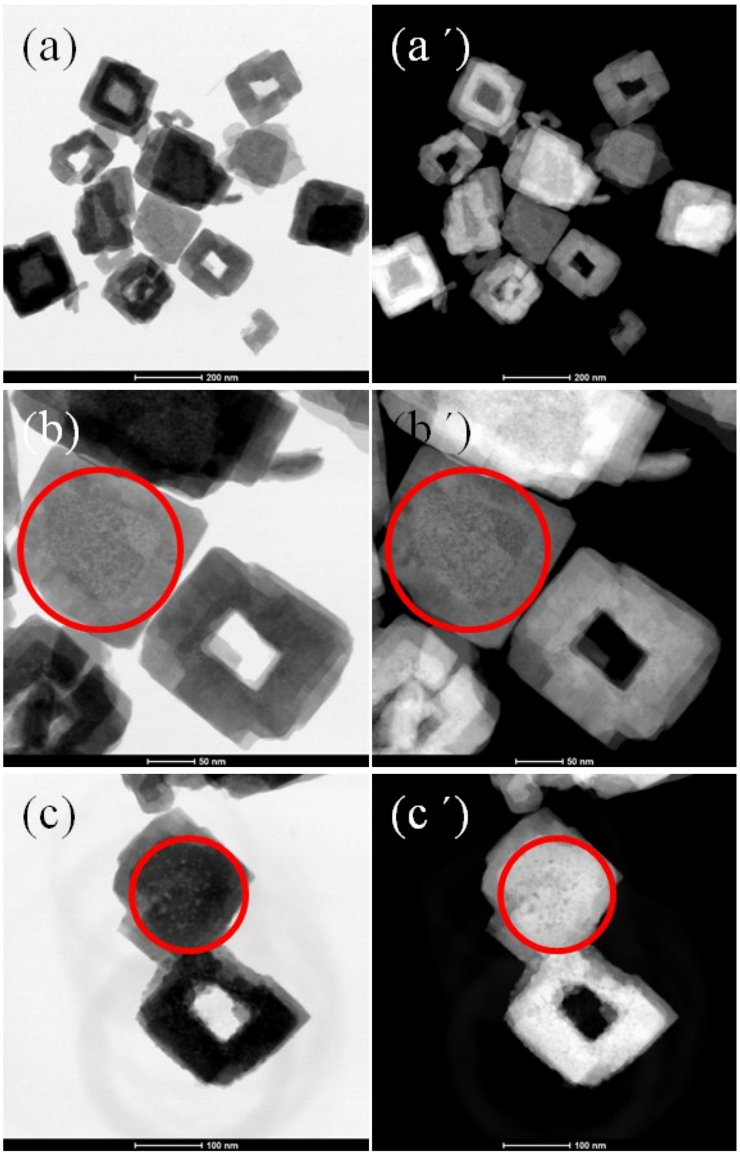

Fig. S10 TEM and high anglar high-angle annular dark-field scanning transmission electron microscopy (HAADF-STEM) images of the samples obtained at 2 h.

When the reaction time is 2 h, nanoplates and nanorings were obtained. As can be seen, holes and irregular small particles were observed at the center of nanoplates before they turning into nanorings, indicating the metastable characteristic of the middle of nanoplates.

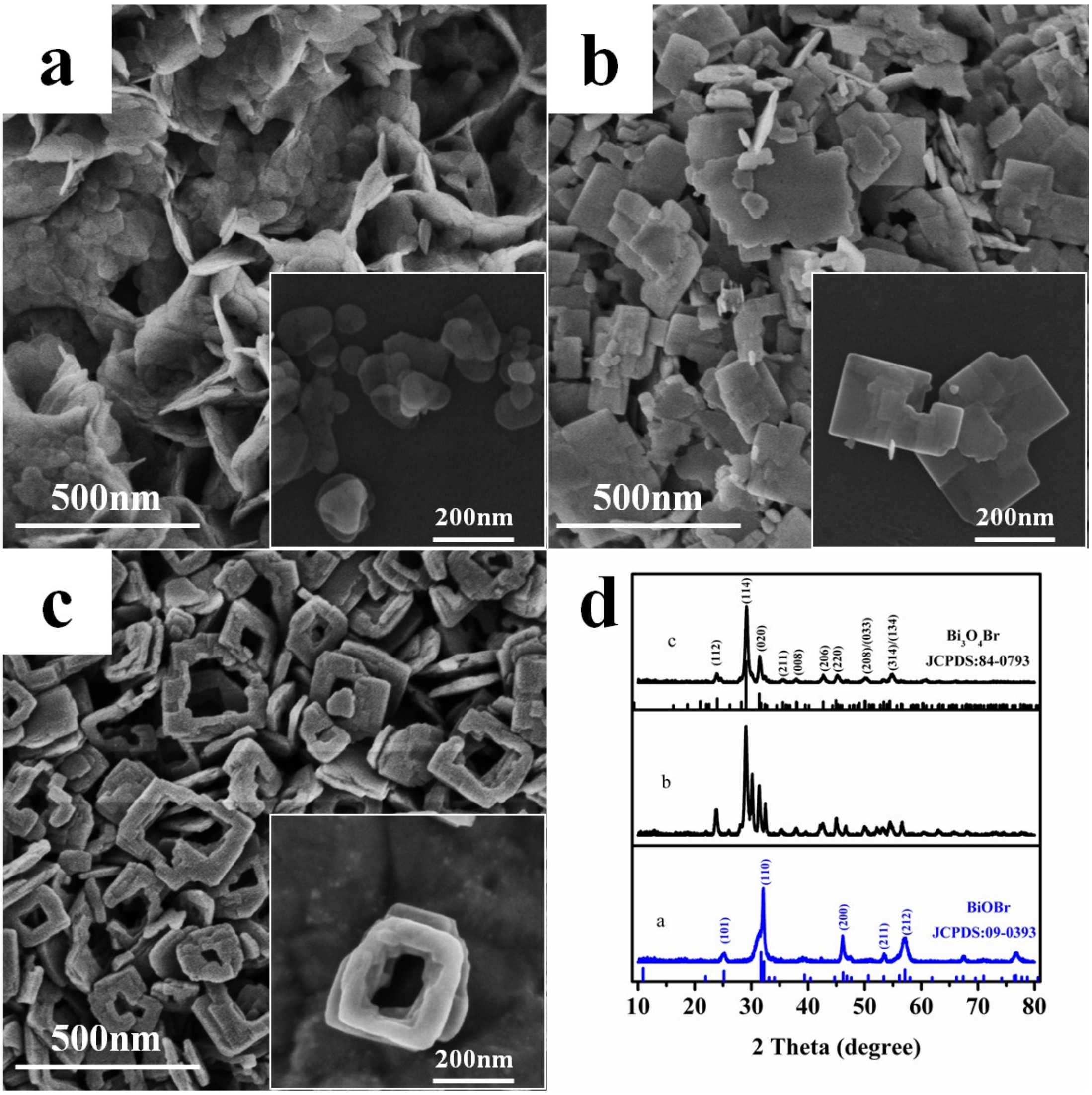

Fig. S11 TEM and XRD images of the samples obtained at 60 ℃. (a) 48 h, (b) 144 h, (c) 196 h (d) the corresponding XRD patterns of the samples.

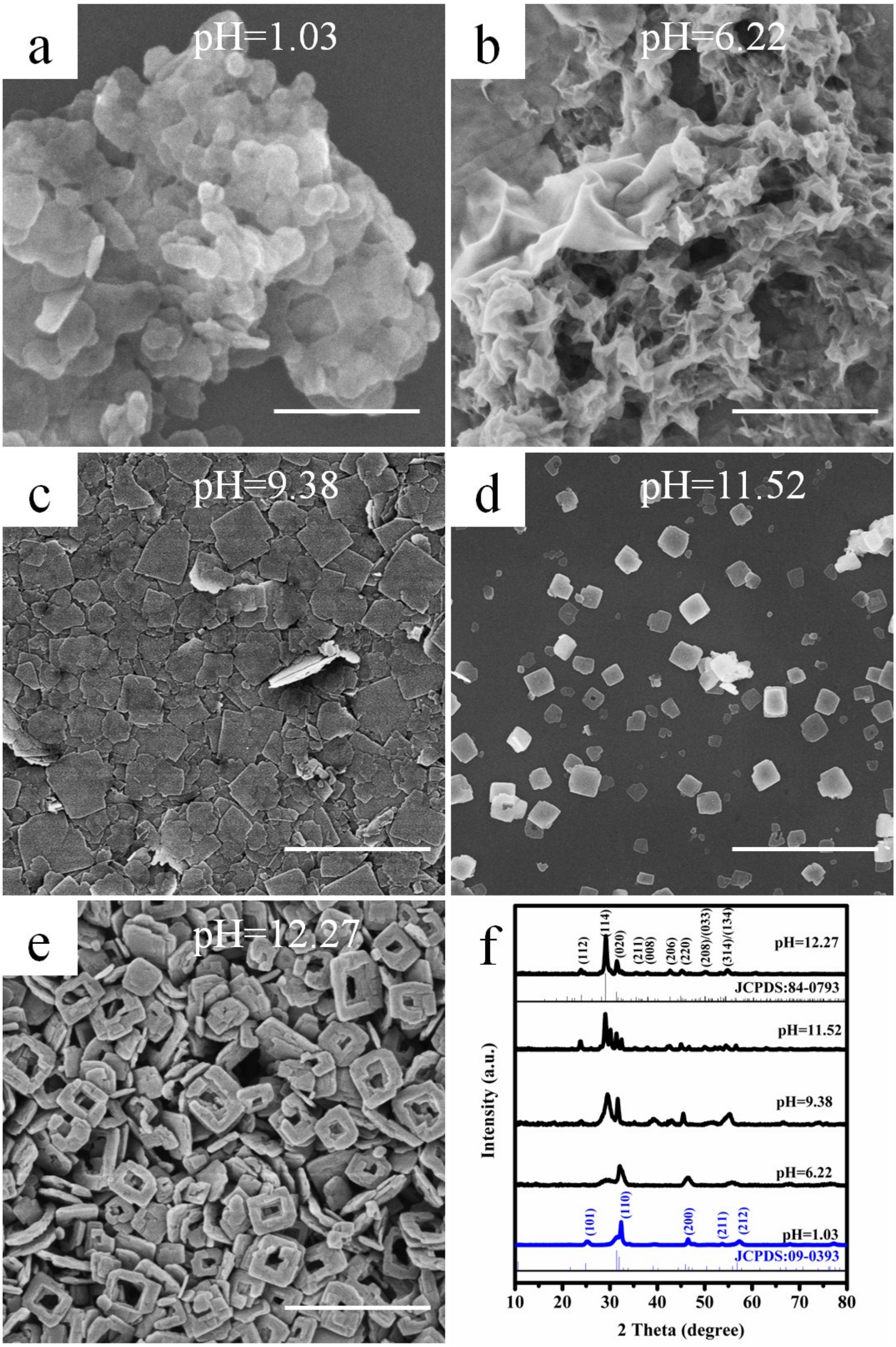

Fig. S12 SEM and XRD images of the as-prepared BOB NRs obtained through the selective etching process with different pH value. a) pH=1.03. b) pH=6.22. c) pH=9.38. d) pH=11.52. e) pH=12.27. f) XRD patterns.

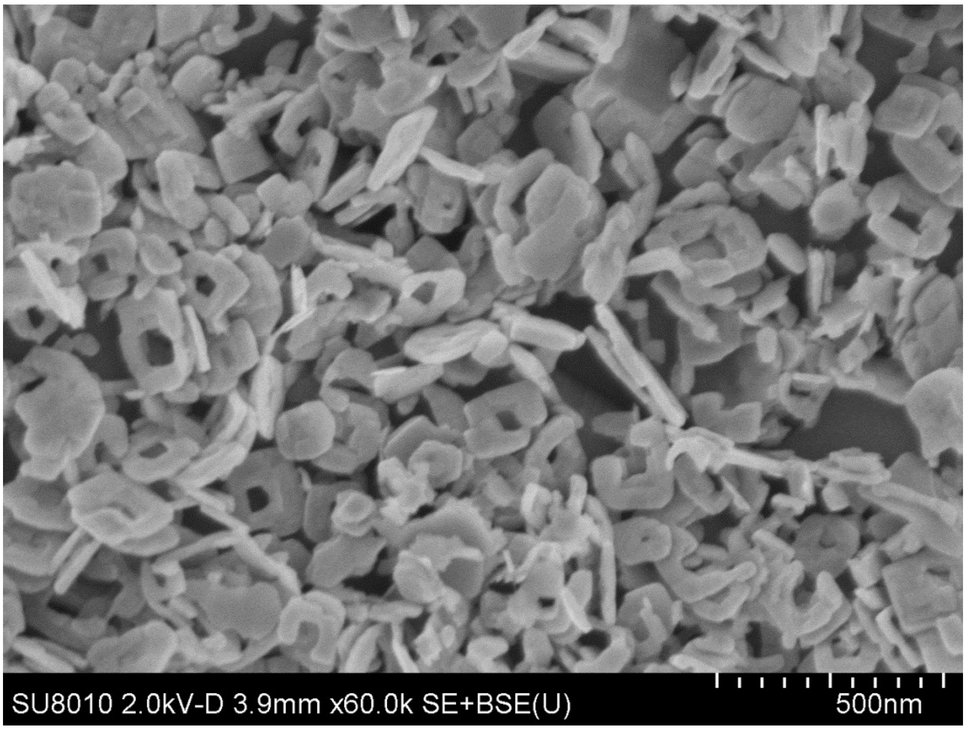

Fig. S13 SEM images of the samples obtained with the same amount of CTAC instead of CTAB. Other reaction parameters are remain unchanged.

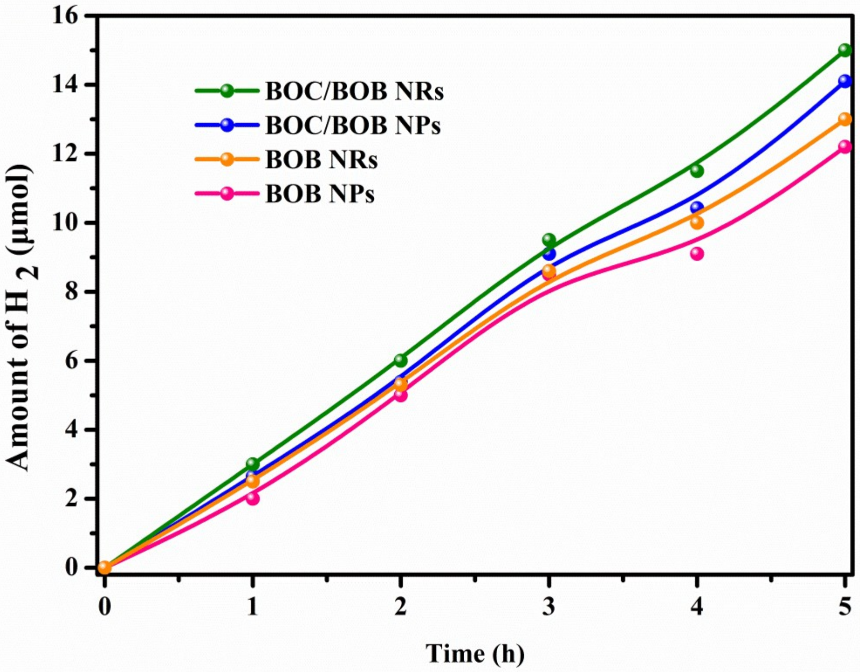

Fig. S14 Hydrogen evolution activities of our as-prepared samples.(The method we used was the same as Jiang’s work) [S2]

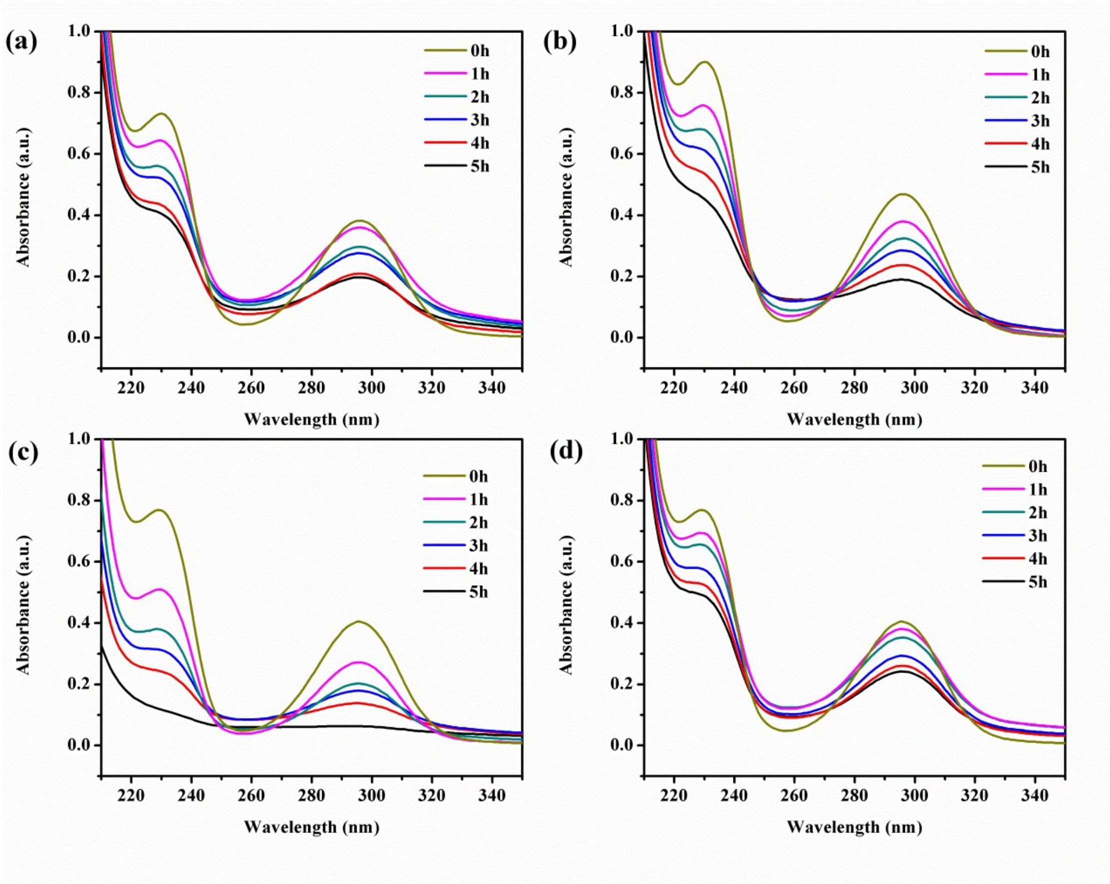

Fig. S15 UV-Vis spectra of the photodegradation of SA by (a) BOC/BOB NPs, (b) BOC/BOB NRs, (c) BOB NRs, (d) BOB NPs.

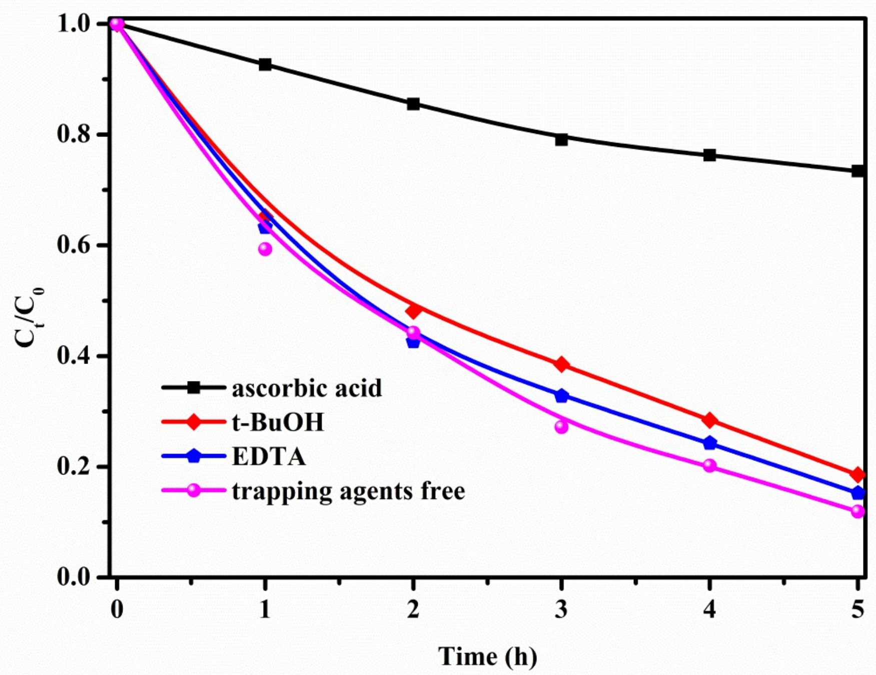

Fig. S16 The photocatalytic activity of BOB NRs with different quenchers. (Ethylene diamine tetra-acetic acid (EDTA, hole scavenger), tert-butanol (t-BuOH, hydroxyl radicals quencher) and ascorbic acid (superoxide quencher)).

As shown in Fig. S16, the SA degradation was significantly suppressed after trapping $\cdot O^{2-}$ by ascorbic acid. When trapping photo-induced holes and OH with EDTA and t-BuOH, the photodegradation rate exhibited much weaker restraining effect. As a result, the $\cdot O^{2-}$ radical was the main active species during the photodegradation process. (The method we used was cited as 37)

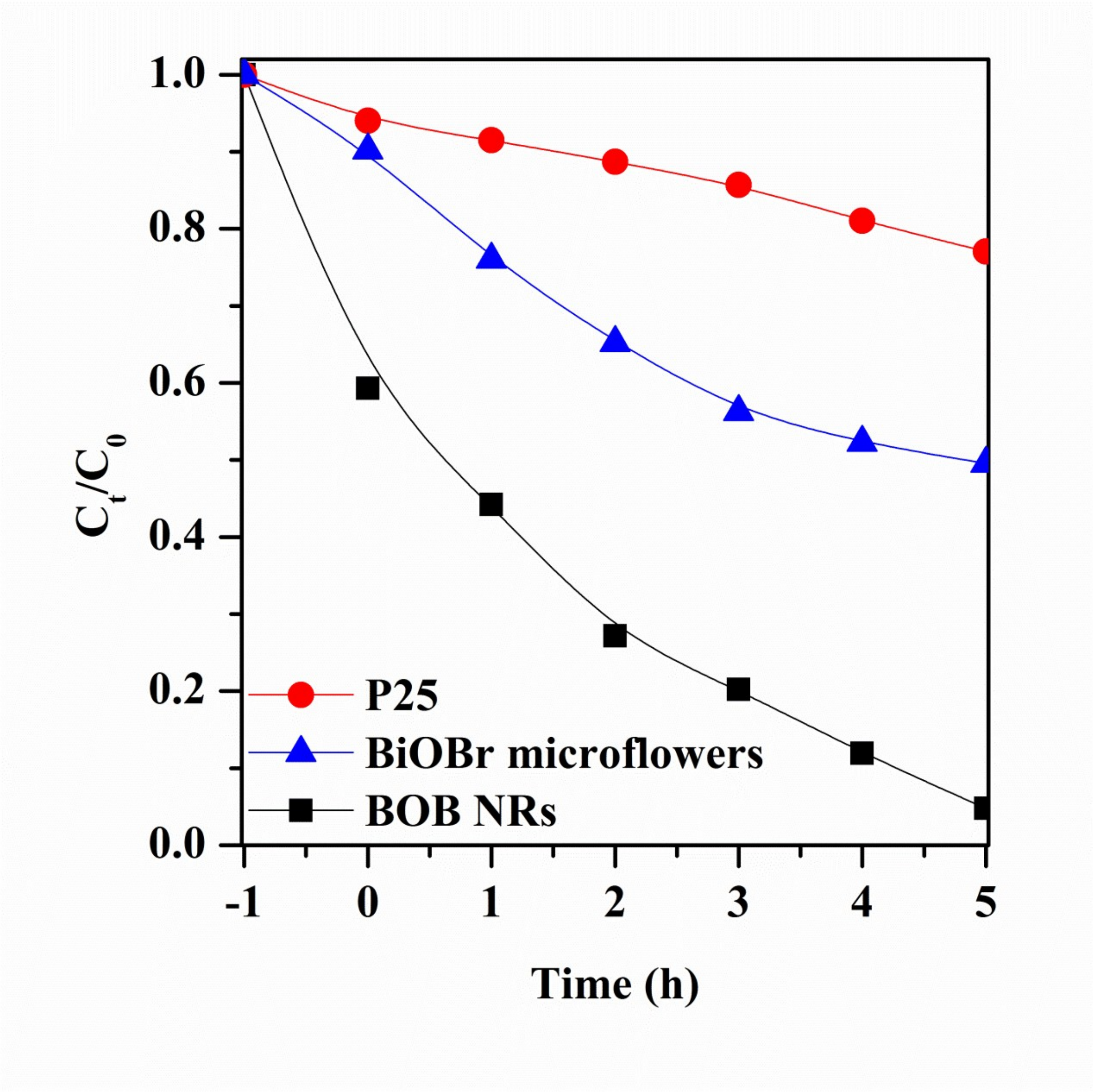

Fig. S17 Photodegradation properties of SA when using BOB NRs, BiOBr microflowers and P25 as the catalysts.

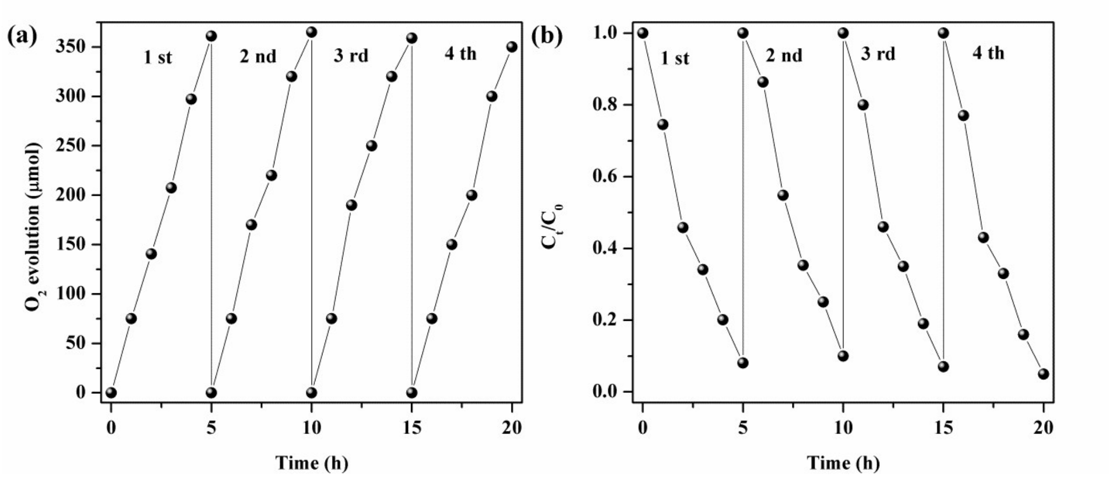

Fig. S18 (a) Repeatable oxygen evolution performance and (b) repeatable SA degradation performance of BOB NRs.

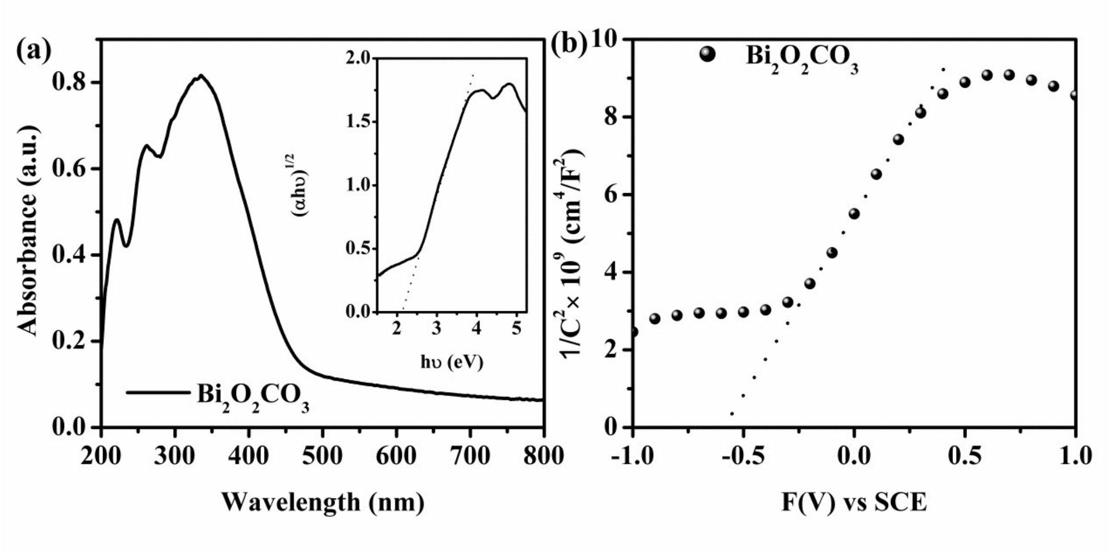

Fig. S19 DRS and Mott-schottky plots of $Bi_2O_2CO_3$ (prepared without adding CTAB in our experiment).

In order to explore the band structures of the hybrid samples, we carefully examined the band gaps and conductive potential of $Bi_2O_2CO_3$ species since the corresponding datas of Bi_3O_4Br were shown in Fig. 7. From Fig S19a, the band gap of $Bi_2O_2CO_3$ is about 2.0 eV. The MS plots of $Bi_2O_2CO_3$ displayed positive slope, revealing the n-type characteristic of $Bi_2O_2CO_3$. The FB level of $Bi_2O_2CO_3$ is -0.62 eV VS SCE, CB is -0.72 eV VS SCE (-0.49 eV VS NHE).

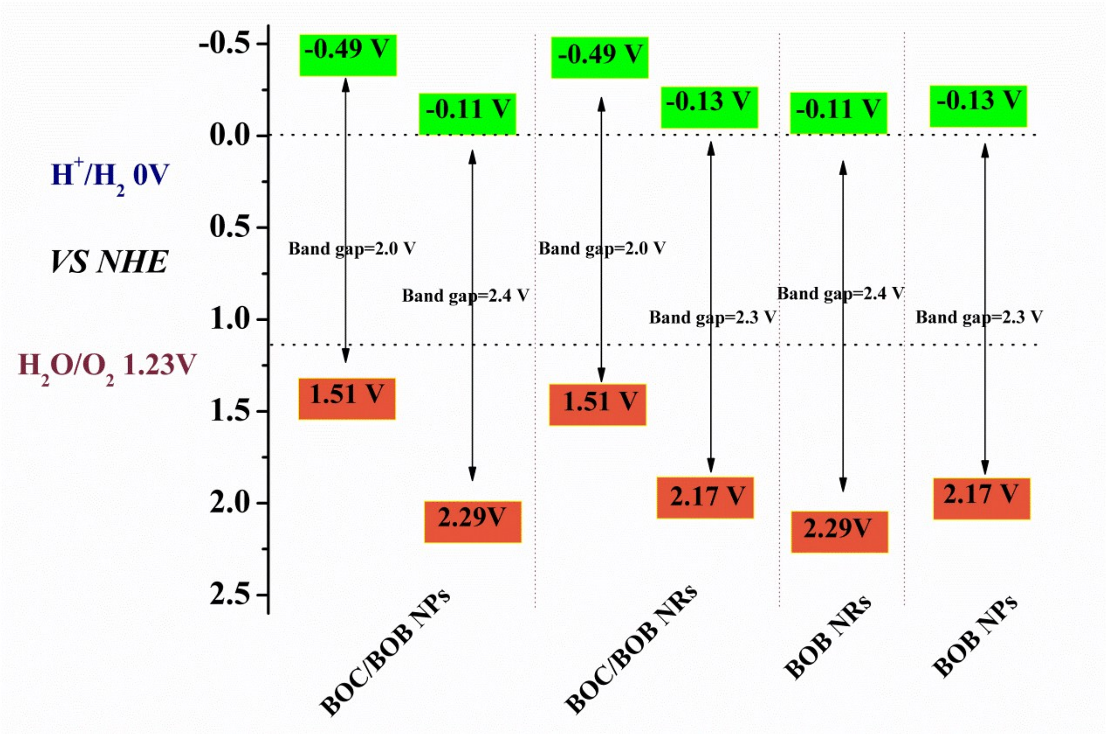

Fig. S20 Band structures of these samples.

The band gaps were calculated via DRS measurement, and the CB values of the samples were dirived from the FB potentials from MS plots (about -0.1-0.3 eV difference). Notably, SCE are reference in our experiment, thus we normalize our datas from SCE to NHE by:

$$E_{NHE}=E_{SCE}+0.23+0.059\ pH$$

Finally, the detailed datas were shown in Fig. S20. The band structures of hybrid species were complex, since the n-n juctuion between $Bi_2O_2CO_3$ and Bi_3O_4Br was different from the traditional p-n junction which exhibits same Femi level in both species. But, our calculation could possibily express the band structures of hybrid BOC/BOB NRs and BOC/BOB NPs.

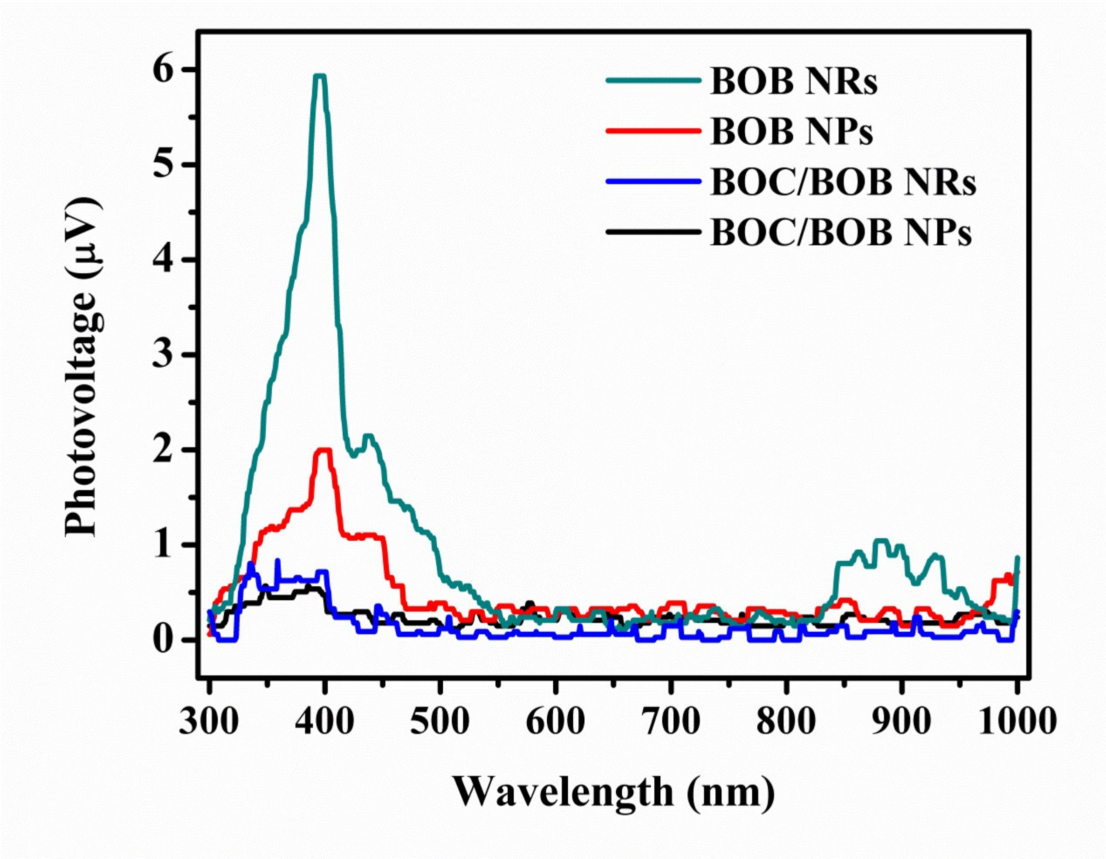

Fig. S21 SPV spectroscopy of the as-prepared samples.

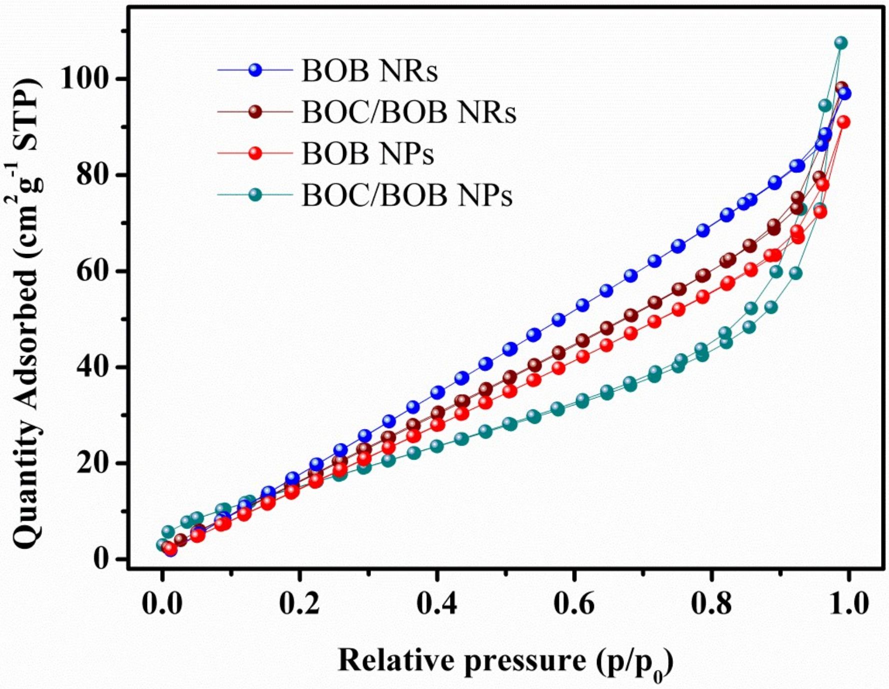

Fig. S22 BET specific surface area of as-prepared samples.

The detailed BET specific area of the BOC/BOB NPs, BOC/BOB NRs, BOB NRs and BOB NPs was 98.02, 98.40, 101.83 and 65.28 m^2 g^{-1}, respectively. As shown in Fig. S22, nanorings also possessed the larger BET surface area than the nanoplates. Thus, the ringlike structures might exhibit better adsorption capacities than nanoplates.